International Journal of Engineering and Information Systems (IJEAIS)
ISSN: 2643-640X
Vol. 6 Issue 8, August - 2022, Pages: 27-49

Numerical Simulation of Natural Convection in a Sinusoidal Corrugated Enclosure with an Inner Circular Cylinder Filled with Ag-Nanofluid Superposed Porous Layers

Salam Hadi Hussain [1,*], Mustafa Salah Rahomey[2] and Basil Mahdi Al-Srayyih[2]

[1]Department of Automobile Engineering, College of Engineering-Al Musayab, University of Babylon, Babylon Province, Iraq
[2]Department of Mechanical Engineering, College of Engineering, University of Babylon, Babylon Province, Iraq
*Corresponding Author Email Addresses: salamphd1974@yahoo.com or met.salam.hadi@uobabylon.edu.iq
Co-author Email: mustafa.rahomey@yahoo.com

Abstract: *Natural convection flows inside an enclosure partly filled by a vertical porous slab saturated with Ag-water nanofluid under the effects of an inner heated circular cylinder and a corrugated sidewall has been numerically investigated. The enclosure is uniformly heated with a constant temperature, T_h at the surface of the inner cylinder fixed at the enclosure centre and cooled at the enclosure walls with a constant temperature, T_c. The porous slab is located on the left close to the vertical corrugated wall while the fluid layer is located on the right close to the vertical flat wall. The selected domain produced a different behaviour in the flow and heat transfer compared to the enclosures that were used in the previous literature. It has been concluded that there was a significant increase in the heat transfer rate recorded with increasing the Rayleigh number for different values of Darcy number. The lower value of the Darcy number can be overcome by increasing the nanoparticle volume fraction producing a relative enhancement of the heat transfer rate. The lower value of K_r produced a higher heat transfer rate for different Darcy numbers. A significant increase was recorded in the heat transfer rate when $\lambda = 2$ and $Am = 0.2$.*

Keywords: Natural convection, porous-nanofluid layers, corrugated (wavy), hollow enclosure.

Nomenclatures

Am	wave Amplitude	θ	dimensionless temperature
C_p	specific heat at constant pressure (J/kg. K)	λ	Wave frequency
Da	Darcy number (K/L^2)	μ	Absolute viscosity, (Pa.sec)
g	gravitational acceleration (m/s^2)	π	Mathematical constant, (3.14159)
k	thermal conductivity W/ (m. K)	ρ	Density, (kg/m^3)
K	porous medium permeability (m^2)	υ	kinematic viscosity, (m^2/sec)
L	side length of enclosure (m)	ϕ	nanoparticles volume fraction
n	normal vector on a plane	Ψ	stream function, ($m^2.s^{-1}$)
Nu	Nusselt number	Ψ	dimensionless stream function, (ψ/α)
p	pressure, (Pa)	Subscripts	
P	dimensionless pressure	av	average
Pr	Prandtl number	c	cold
r	cylinder radius (m)	h	hot
Ra	Rayleigh number, $Ra = \frac{g\beta_f L^3 \Delta T}{\nu_f \alpha_f}$	l	local
Rk	thermal conductivity ratio = kp/kna	na	nanofluid

T	Temperature (Kelven)	o	reference point
u	velocity component along x-direction, (m/sec)	p	porous
v	velocity component along y-direction, (m/sec)	pa	nanoparticles
U	Dimensional velocity component in x-direction	w	water
V	Dimensional velocity component in y-direction		
x, y	Cartesian coordinates (m)		
X,Y	dimensionless Cartesian coordinates		
Greek symbols			
α	thermal diffusivity, (m^2/sec)		
β	thermal expansion coefficient, (1/Kelven)		
ζ			
η			

1. Introduction

The study of natural convection inside enclosures using various types of heat transfer controlling techniques has been widely presented over the last few years; it represents a base for developing modern industrial engineering technology. Convective heat transfer inside enclosures has been investigated in many literatures by using different thermal boundary conditions and heat transfer controlling techniques such as porous media, nanofluid, magnetic field (MHD) and corrugated wall. It is simulated inside different shapes of physical domains by using the Computational Fluid Dynamics (CFD) in different numerical solution methods. CFD has been helped the researchers and designers for extensive simulation and analysis to reduce the manufacturing cost and optimize the design of the thermal system.

The investigation of natural convection flow inside an enclosure using a porous medium is an important issue in many industrial engineering applications such as ground-coupled heat pumps, solar collectors, heat exchangers, cooling of electronic equipment [1]. The convective heat transfer rate is enhanced by using the porous medium in recent years [2]–[4]. This stems from that the porous medium has the ability to draw the heat from the source by the conduction mode beside the random movement of the fluid flow through it that causes to an increase the heat exchange between the fluid and the porous medium by the convection mode [5]. Interesting details about the porous media can be found in the reference books [6]–[8].

Many studies investigated the convective heat transfer in enclosures filled with a porous medium saturated with a single-phase fluid. Several important studies [9]–[13] investigated the natural convection flow inside a porous enclosure saturated with a single-phase fluid. Basak et al. [14] used various thermal boundary conditions at the enclosure boundaries to investigate the steady-state natural convection flow inside a square enclosure entirely filled by a porous medium saturated with a single-phase fluid. They found that a high value of the Rayleigh number and Darcy number caused higher heat transfer rates due to an increase in the circulation strength and flow penetration through the porous medium, respectively.

Another approach for controlling and enhancing the convective heat transfer is named nanofluid. Nanofluid is a single-phase fluid that contains a suspension of nanoparticles in a size of 100 nm. Researchers found that nanofluid can be enhanced the convective heat transfer compared to the single-phase fluid depending on the volume fraction, type and size of the added nanoparticles to the single-phase fluid. This is attributed to the fact that the thermal conductivity property of the nanoparticles is greater than that of the single-phase fluid. Steady-state laminar natural convection flows within an enclosure partly filled by a porous medium saturated with a nanofluid under the effect of differentially heated walls of a square enclosure was presented by [4], [15]–[18]. Al-Srayyih et al.[17] found that the heat transfer rates were enhanced in the presence of copper-water nanofluid compared to the single-phase fluid (water). In addition, the heat transfer rates were enhanced at lower values of the thermal conductivity ratio ($kp/kna \leq 1$) and the porous layer thickness ($Xp \leq 0.3$) when Darcy number ($Da \leq 10^{-3}$) for all values of Rayleigh number.

In addition to using the porous medium and the nanofluid as controlling techniques for the heat transfer inside enclosures (related to the present study), the corrugated walls of an enclosure can be used to enhance the heat transfer rate in many industrial engineering applications such as in underground cable systems, flat-plate solar collectors and cooling systems of micro-electronic devices [19]. Many studies, such as [20]–[24] have been devoted to the effect of irregular enclosure surfaces on convective heat transfer in different thermal boundary conditions. These enclosures were filled with a nanofluid or a porous medium saturated with a single-phase fluid or nanofluid. Sojoudi et al.[21] numerically studied the unsteady natural convection flow inside a porous enclosure saturated with a single-phase fluid under the effect of sinusoidal corrugated vertical side-walls. They concluded that the heat transfer increased with increasing the Rayleigh number. The higher corrugation amplitude produced a higher heat transfer rate compared to the corrugation wave number.

The use of a cylinder inside an enclosure causes a new trend of convective heat transfer compared to the above-mentioned literature, where the fluid particles pass around the cylinder causing flow splitting within the enclosure. Several interesting studies [25]–[30] investigated the natural convection flow inside enclosures containing inner circular cylinders with various thermal boundary conditions using a single-phase fluid. Hussain and Hussein [27] studied the natural convection flow inside a square enclosure heated by an inner circular cylinder using a single-phase fluid (air). The investigation range of the Rayleigh number was 10^3-10^6, while the location of the inner heated circular cylinder was changed vertically along the centerline of the enclosure from -0.25L to 0.25L. They concluded that the heat transfer rate of the cold surfaces of the square enclosure was non-linearly behaved depending on the inner cylinder locations with increasing Rayleigh number. Roslan et al. [31] studied the convective heat transfer within a two-dimensional square enclosure filled with a nanofluid under the effect of an inner fixed and cooled rotating circular cylinder by using the Galerkin Finite Element Method (GFEM). Ravnik [32] numerically studied the comparison of two and three- dimensional simulations of the effects of heated circular and elliptical cylinders on the natural convection inside a cooled cubical enclosure using

Al_2O_3, Cu and TiO_2 nanofluids. Mixed convection and entropy generation in a two–dimensional wavy enclosure filled with a nanofluid under the effects of rotating an inner circular cylinder and the partially heated bottom wall of the enclosure was investigated by [33]. The effect of a rotating cooled circular cylinder on the mixed convection flow inside a two-dimensional enclosure partly filled by a horizontal porous slab saturated with a single-phase fluid was presented in [34]. Hussain and Rahomey [35] numerically studied the nanofluid natural convection flow in a square enclosure partly filled by a vertical porous slab saturated with Ag-nanofluid by comparing an inner circular cylinder with different other geometries of cylinders. The inner cylinder was subjected to a hot temperature, while the enclosure walls were isothermally cooled. It was found that the heat transfer rate along the enclosure wall surfaces in the presence of a triangular inner cylinder was better compared to other geometries. In addition, increasing the porous layer thickness from 0.2 to 0.8 led to a significant decrease in the convective heat transfer to about 50% due to increasing the resistance area of the porous matrix. The combination of the selected heat transfer controlling techniques in the present study was investigated by [36]. Hussein et al.[36] numerically studied the mixed convection of a two-dimensional trapezoidal enclosure partially filled by a horizontal porous layer saturated with a CuO-nanofluid under the effect of a rotating inner circular cylinder and a bottom heated wavy wall of the enclosure attached to the porous layer using GFEM. It was found that the heat transfer rate increased when the Rayleigh and Darcy numbers, the nanoparticle volume fraction, the inner radius and the angular rotational velocity of the inner cylinder increased, while it decreased with increasing the porous layer thickness and the corrugated wall frequency.

Despite the fact that the mentioned important investigations have been widely presented in the study of convective heat transfer using various types of heat transfer controlling techniques and thermal boundary conditions, there is a lack of information on the characteristics of laminar natural convection inside a vertical corrugated enclosure partly filled with a porous vertical slab saturated with a nanofluid under the effect of an inner heated cylinder. These investigations have helped to motivate the present study to obtain new simulation results using the characteristics of the porous medium, the nanofluid and the corrugated wall. The inner heated circular cylinder and a corrugated left wall of an enclosure partly filled with a porous medium saturated with a nanofluid produces a different trend of the flow and heat transfer compared to the enclosures that were used in the previous literature. Accordingly, no work has yet been done to study the effect of an inner heated circular cylinder on natural convection flow inside a corrugated enclosure partly filled with a vertical porous slab saturated with a nanofluid. This study may be engaging in many industrial engineering applications of modern technology.

2. Mathematical formulation and solution procedure

Laminar natural convection is modelled in a two-dimensional hollow square enclosure with length L, partially filled with a porous slab saturated by nanofluid and the same nanofluid filled the remainder of the enclosure, as shown schematically in Figure 1. A circular cylinder with radius (r = 0.2 L) is fixed in the centre of the enclosure. It is isothermally heated while the enclosure walls are isothermally cooled. The differentially heated between the cylinder circumference and enclosure walls causes to develop the fluid flow inside the enclosure due to the temperature difference. This causes to occur that the density gradient (due to temperature gradient) is radial and the gravity vector acts perpendicularly, where the circulation inside the enclosure depends on theses vector orientation. The left wall of the enclosure is considered as a corrugated (sinusoidal) wall. The porous slab and nanofluid layer are simulated as having thicknesses X_p and $L - X_p$, respectively. The interface between them is assumed permeable with no-slip condition, while the enclosure walls are impermeable with no-slip condition. The selected nanofluid is consist of a single-phase fluid (water) and (Ag) nanoparticles. It is assumed as a homogeneous mixture in thermal equilibrium with no-slip velocity between the single- phase and the nanoparticles. The nanofluid properties are illustrated in Table 1.

Table (1) Thermo-physical properties of single- phase (water) and silver nanoparticle [18].

Properties	Pure water	silver (Ag)
Cp(J/kg.K)	4179	235
k (W/m.K)	0.613	429
$\rho(kg/m^3)$	997.1	10500
$\beta(1/K)\times10^{-5}$	21	1.89

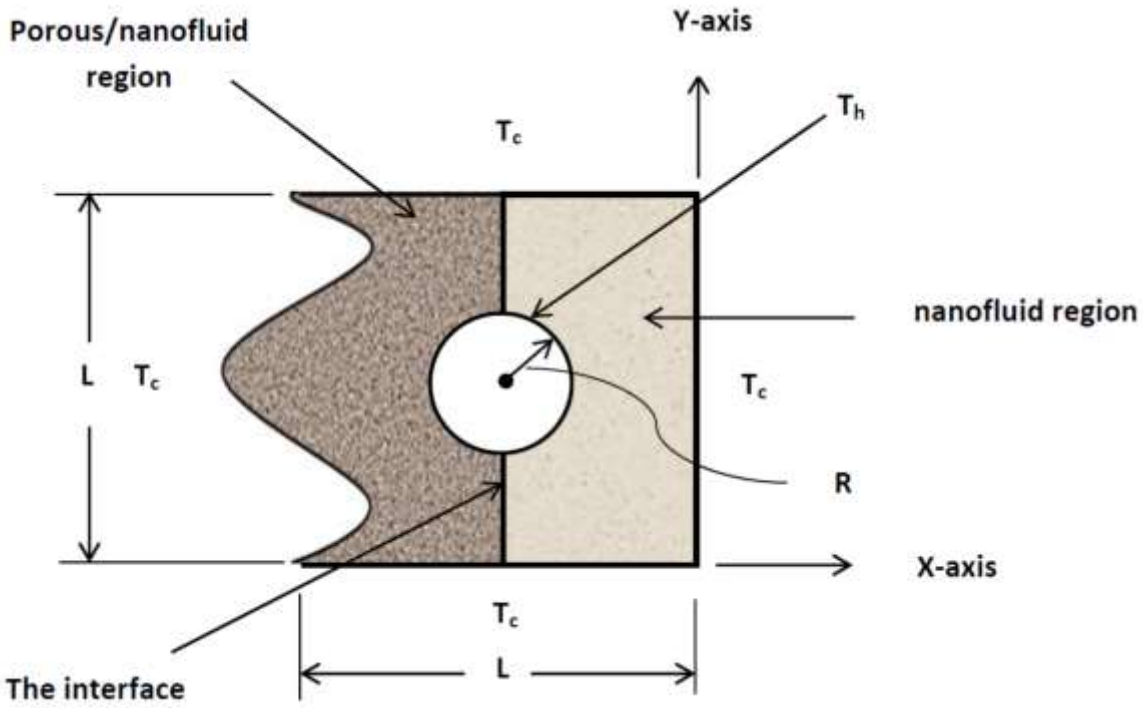

Figure 1: Physical domain with coordinate system and the boundary conditions.

The flow is assumed steady, laminar and incompressible with constant physical properties except the density that is considered to vary with temperature according to the Boussinesq approximation. The concept of Boussinesq approximation states that when a small variation occurs in the density of fluid particles due to a temperature difference, this variation can be neglected except when it is considered with the gravitational acceleration (g). The Boussinesq approximation can be expressed [8]

$$\rho_f = \rho_o[1 - \beta_{th}(T_f - T_o)] \quad (1)$$

The Navier-Stokes model is used to simulate the natural convection flow for the nanofluid layer while the Darcy–Brinkman model is assumed to solve the governing equations in the porous slab. The radiation mode and the internal heat generation are assumed negligible.

Accordingly, the dimensional governing equations for the nanofluid layer and porous slab can be written as follows:[35]:

For nanofluid layer:

$$\frac{\partial(u)_{na}}{\partial x}+\frac{\partial(v)_{na}}{\partial y}=0 \quad (2)$$

For porous slab:

$$(u)_{na}\frac{\partial(u)_{na}}{\partial x}+(v)_{na}\frac{\partial(u)_{na}}{\partial y}=-\frac{1}{(\rho)_{na}}\frac{\partial p}{\partial x}+\frac{(\mu)_{na}}{(\rho)_{na}}\left(\frac{\partial^2(u)_{na}}{\partial x^2}+\frac{\partial^2(u)_{na}}{\partial y^2}\right) \quad (3)$$

$$(u)_{na}\frac{\partial(v)_{na}}{\partial x}+(v)_{na}\frac{\partial(v)_{na}}{\partial y}=-\frac{1}{(\rho)_{na}}\frac{\partial p}{\partial y}+\frac{(\mu)_{na}}{(\rho)_{na}}\left(\frac{\partial^2(v)_{na}}{\partial x^2}+\frac{\partial^2(v)_{na}}{\partial y^2}\right)+(\beta)_{na}g((T)_{na}-(T)_c) \quad (4)$$

$$(u)_{na}\frac{\partial(T)_{na}}{\partial x}+(v)_{na}\frac{\partial(T)_{na}}{\partial y}=(\alpha)_{na}\left(\frac{\partial^2(T)_{na}}{\partial x^2}+\frac{\partial^2(T)_{na}}{\partial^2 y}\right) \quad (5)$$

The dependent and independent parameters to transform the equations (2-9) to the

$$\frac{\partial(u)_{na}}{\partial x}+\frac{\partial(v)_{na}}{\partial y}=0 \quad (6)$$

$$(u)_{na}\frac{\partial(u)_{na}}{\partial x}+(v)_{na}\frac{\partial(u)_{na}}{\partial y}=-\frac{1}{(\rho)_{na}}\frac{\partial p}{\partial x}+\frac{(\mu)_{na}}{(\rho)_{na}}\left(\frac{\partial^2(u)_{na}}{\partial x^2}+\frac{\partial^2(u)_{na}}{\partial y^2}\right)-\frac{(\mu)_{na}}{(\rho)_{na}K}(u)_{na} \quad (7)$$

$$(u)_{na}\frac{\partial(v)_{na}}{\partial x}+(v)_{na}\frac{\partial(v)_{na}}{\partial y}=-\frac{1}{(\rho)_{na}}\frac{\partial p}{\partial y}+\frac{(\mu)_{na}}{(\rho)_{na}}\left(\frac{\partial^2(v)_{na}}{\partial x^2}+\frac{\partial^2(v)_{na}}{\partial y^2}\right)-\frac{(\mu)_{na}}{(\rho)_{na}K}(v)_{na}+(\beta)_{na}g((T)_{na}-(T)_c) \quad (8)$$

$$(u)_{na}\frac{\partial(T)_{na}}{\partial x}+(v)_{na}\frac{\partial(T)_{na}}{\partial y}=(\alpha)_{na}\left(\frac{\partial^2(T)_{na}}{\partial x^2}+\frac{\partial^2(T)_{na}}{\partial y^2}\right) \quad (9)$$

dimensionless equations form can be written as follows [35]:

$$X=\frac{x}{L},\ Y=\frac{y}{L},\ U=\frac{uL}{(\alpha)_w},\ V=\frac{vL}{(\alpha)_w},\ P=\frac{PL}{(\rho)_w\times((\alpha)_w)^2},\ \Psi=\frac{\psi}{(\alpha)_w},$$

$$(\theta)_{na}=(\theta)_p=\frac{(T)_{na}-(T)_c}{(T)_h-(T)_c},\ Ra=\frac{(\beta)_w\times g\times\Delta T\times L^3}{(\vartheta)_w\times(\alpha)_w},\ Pr=\frac{(\vartheta)_w}{(\alpha)_w},\text{ and } Da=\frac{K}{L^2} \quad (10)$$

The relations between the single-phase

fluid and the nanoparticles to perform the nanofluid are as follows [35]:

$$(\rho)_{na}=(1-\phi)(\rho)_{na}+\phi(\rho)_{pa} \quad (11)$$

$$(\mu)_{na}=\frac{(\mu)_w}{(1-\phi)^{2.5}} \quad (12)$$

The thermal diffusivity ratio and the effective

$$(\rho Cp)_{na}=(1-\phi)(\rho Cp)_w+\phi(\rho Cp)_{pa} \quad (13)$$

$$(\beta)_{na}=(1-\phi)(\rho\beta)_w+\phi(\rho\beta)_{pa} \quad (14)$$

$$(\rho\beta)_{na}=(1-\phi)\rho_w+\phi\rho_{pa} \quad (15)$$

$$(k)_{na}=\frac{((k)_{pa}+2(k)_w)-2\phi((k)_w-(k)_{pa})}{((k)_{pa}+2(k)_w)+\phi((k)_w-(k)_{pa})}(k)_w \quad (16)$$

dimensionless thermal conductivity are as follows

$$\alpha_{na}=\frac{k_{na}}{(\rho C_P)_{na}},\ (k)_{eff}=Rk*\frac{(k)_{na}}{(k)_w} \quad (17)$$

Accordingly, using the parameters in equation (10) and the thermo-physical properties of the nanofluid in equations (11-16) and equation (17), the dimensionless governing equations can be written in terms of the nanoparticles' volume fraction as follows [35]:

For nanofluid layer:

$$\frac{\partial(U)_{na}}{\partial X}+\frac{\partial(V)_{na}}{\partial Y}=0 \quad (18)$$

For porous slab

$$(U)_{na}\frac{\partial(U)_{na}}{\partial X}+(V)_{na}\frac{\partial(U)_{na}}{\partial Y}=-\frac{\partial P}{\partial X}+\frac{(\rho)_w}{(\rho)_{na}\times(1-\phi)^{2.5}}\times Pr\times\left(\frac{\partial^2(U)_{na}}{\partial X^2}+\frac{\partial^2(U)_{na}}{\partial Y^2}\right) \quad (19)$$

$$(U)_{na}\frac{\partial(V)_{na}}{\partial X}+(V)_{na}\frac{\partial(V)_{na}}{\partial Y}=-\frac{\partial P}{\partial Y}+\frac{(\rho)_w}{(\rho)_{na}\times(1-\phi)^{2.5}}\times Pr\times\left(\frac{\partial^2(V)_{na}}{\partial X^2}+\frac{\partial^2(V)_{na}}{\partial Y^2}\right)+\frac{(\rho\beta)_{na}}{(\rho)_{na}\times(\beta)_w}\times Pr.Ra.(\theta)_{na} \quad (20)$$

2.1 Boundary conditions

$$(U)_{na}\frac{\partial(\theta)_{na}}{\partial X}+(V)_{na}\frac{\partial(\theta)_{na}}{\partial Y}=\left(\frac{(\alpha)_{na}}{(\alpha)_w}\right)\times\left[\left(\frac{\partial^2(\theta)_{na}}{\partial X^2}+\frac{\partial^2(\theta)_{na}}{\partial Y^2}\right)\right] \quad (21)$$

The boundary conditions for each case (flat and corrugated left wall of the enclosure) are:

$$\frac{\partial(U)_{na}}{\partial X}+\frac{\partial(V)_{na}}{\partial Y}=0 \quad (22)$$

$$(U)_{na}\frac{\partial(U)_{na}}{\partial X}+V\frac{\partial(U)_{na}}{\partial Y}=-\frac{\partial P}{\partial X}+\frac{(\rho)_w}{(\rho)_{na}\times(1-\phi)^{2.5}}.Pr\left(\frac{\partial^2(U)_{na}}{\partial X^2}+\frac{\partial^2(U)_{na}}{\partial Y^2}\right)-\frac{(\rho)_w}{(\rho)_{na}\times(1-\phi)^{2.5}}.\frac{Pr}{Da}.(U)_{na} \quad (23)$$

$$(U)_{na}\frac{\partial(V)_{na}}{\partial X}+(V)_{na}\frac{\partial(V)_{na}}{\partial Y}=-\frac{\partial P}{\partial Y}+\frac{(\rho)_w}{(\rho)_{na}\times(1-\phi)^{2.5}}\times Pr\left(\frac{\partial^2(V)_{na}}{\partial X^2}+\frac{\partial^2(V)_{na}}{\partial Y^2}\right)+\frac{(\rho\times\beta)_{na}}{(\rho)_{na}\times(\beta)_w}\times Pr.Ra.(\theta)_{na}-\frac{(\rho)_w}{(\rho)_{na}\times(1-\phi)^{2.5}}\times\frac{Pr}{Da}(V)_{na} \quad (24)$$

$$(U)_{na}\frac{\partial(\theta)_p}{\partial X}+(V)_{na}\frac{\partial(\theta)_p}{\partial Y}=\left(\frac{(\alpha)_{na}}{(\alpha)_w}\right)*\left[\left(\frac{\partial^2(\theta)_p}{\partial X^2}+\frac{\partial^2(\theta)_p}{\partial Y^2}\right)\right] \quad (25)$$

At the outer boundaries of the enclosure $\Psi = 0, \theta = 0$ (26)

At the circumference of the circular cylinder $\Psi = 0, \theta = 1$ (27)

The interface between the porous slab and the nanofluid layer is considered permeable with matching values of normal and shear stress, normal and tangential velocities and the temperature of the nanofluid is as a local thermal equilibrium (LTE) with the solid matrix of the porous slab as follows [17]:

$$(\mu)_P=(\mu)_{na},\ (\theta)_p=(\theta)_{na},\ (\psi)_p=(\psi)_{na} \text{ and } \frac{\partial(\theta)_{na}}{\partial X}=Rk\frac{\partial(\theta)_p}{\partial X} \quad (28)$$

2.2 Stream function and Nusselt number

2.2.1 Stream function

The flow inside the porous slab and the nanofluid layer can be simulated by the stream function ψ as a function of U and V velocity components as follows [17]:

$$(U)_{na}=\frac{\partial(\psi)_{na}}{\partial Y},\ (V)_{na}=-\frac{\partial(\psi)_{na}}{\partial X}, \text{ and} \quad (29)$$

$$\frac{\partial^2(\psi)_{na}}{\partial X^2}+\frac{\partial^2(\psi)_{na}}{\partial Y^2}=\frac{\partial(U)_{na}}{\partial Y}-\frac{\partial(V)_{na}}{\partial X} \quad (30)$$

The negative sign of the stream function ψ refers to a clockwise flow direction, and the positive sign indicates an anti-clockwise flow direction.

2.2.2 Nusselt number

Nusselt number can express the heat transfer along the circumference of the circular cylinder, where the heat conduction is equal to the heat convection. The local and average Nusselt number are defined by the following expressions:

$$Nu = \frac{1}{2\pi}\frac{k_{na}}{k_w}\frac{\partial\theta}{\partial n} \quad (31)$$

$$Nu_{av} = \frac{1}{2\pi}\frac{k_{na}}{k_w}\int_0^{2\pi}\frac{\partial\theta}{\partial n}\,dn \quad (32)$$

$$\frac{\partial\theta}{\partial n} = \sqrt{\left(\frac{\partial\theta}{\partial X}\right)^2 + \left(\frac{\partial\theta}{\partial Y}\right)^2} \quad (33)$$

Where n is the outwards unit normal vector for the hot circumference wall and cold walls.

The dimensionless temperature of the hot circumference circular cylinder should be changed from the Cartesian coordinates (X,Y) to the transform coordinates (ζ,η)

$$Nu = \frac{1}{2\pi}\frac{(k)_{na}}{(k)_w}\sqrt{\left(\frac{\partial\theta}{\partial X}\right)^2 + \left(\frac{\partial\theta}{\partial Y}\right)^2} \quad (34)$$

$$Nu_{av} = \frac{1}{2\pi}\frac{(k)_{na}}{(k)_w}\int_0^{2\pi}\sqrt{\left(\frac{\partial\theta}{\partial X}\right)^2 + \left(\frac{\partial\theta}{\partial Y}\right)^2}\,d\zeta \quad (35)$$

The FEM distribution can be applied as follow:

$$Nu = \frac{1}{2\pi}\frac{(k)_{na}}{(k)_w}\sum_{j=1}^{m}\theta_j\sqrt{\left(\frac{\partial\Phi_j}{\partial X}\right)^2 + \left(\frac{\partial\Phi_j}{\partial Y}\right)^2} \quad (36)$$

$$Nu_{av} = \frac{1}{2\pi}\frac{(k)_{na}}{(k)_w}\sum_{j=1}^{m}\theta_j\int_0^{2\pi}\sqrt{\left(\frac{\partial\Phi_j}{\partial X}\right)^2 + \left(\frac{\partial\Phi_j}{\partial Y}\right)^2}\,d\zeta \quad (37)$$

3. Numerical solution

The finite element method is adopted to solve the dimensionless governing equations (18-25). These equations are combined with the boundary condition equations , where the velocity components and temperature are subjugated to the basis set as shown in Ref. [14]. The coupling between the continuity and momentum equations are implemented by using the SIMPLE algorithm. Depending on the three-point Gaussian quadrature, the integrals of the obtained equations are estimated. In addition, the coefficients of the non-linear residual equations are obtained by using the Newton-Raphson method. An iterative process is implemented to find the final data of the dependent variables (U, V, P, and θ) until it reaches the steady-state values and satisfy the convergence criterion at $\leq 10^{-6}$.

3.1 Validations

In this section, to build the confidence in the results for the present study, the numerical results were compared with previously published studies in two validation tests. Firstly, the prediction of the present results is validated with the results by Hussein [29]. The case of the domain is that a steady convective heat transfer for a hot circular cylinder inside an enclosure using a single-phase fluid (air) as a cooling fluid, as shown in Figure 2. The comparison results of the stream function and isotherms are implemented for Rayleigh number (Ra), Ra = 10^4, vertical location of the cylinder (δ), δ = 0 and angle of inclination (Φ) = 0.

In the second validation study, the domain is that of a two-dimensional laminar flow for steady natural convection inside an enclosure partly filled with a vertical porous medium slab saturated with a nanofluid that was presented by [4] as shown in Figure 3. The left and right walls of the enclosure were subjected to the hot and cold temperatures, respectively, while the horizontal walls were thermally isolated. The investigation of the stream function and isotherms is implemented for Rayleigh number (Ra), Ra = 10^5, Darcy number (Da), Da = 10^{-5}, the aspect ratio (A), A = 1, and the porous slab thickness (Xp), Xp = 0.3. The nanofluid is consist of water and copper nanoparticles at a volume fraction of 0.05. The solid lines refer to the water (ϕ= 0), while the dashed lines indicate the nanofluid (ϕ = 0.05).

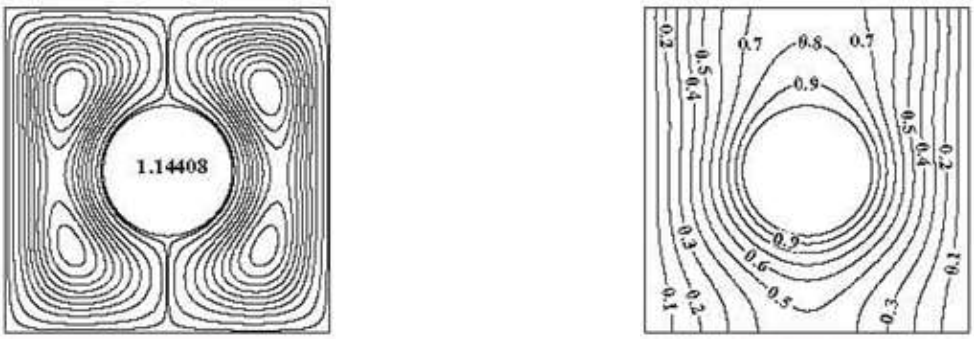

(a) Hussein [29]

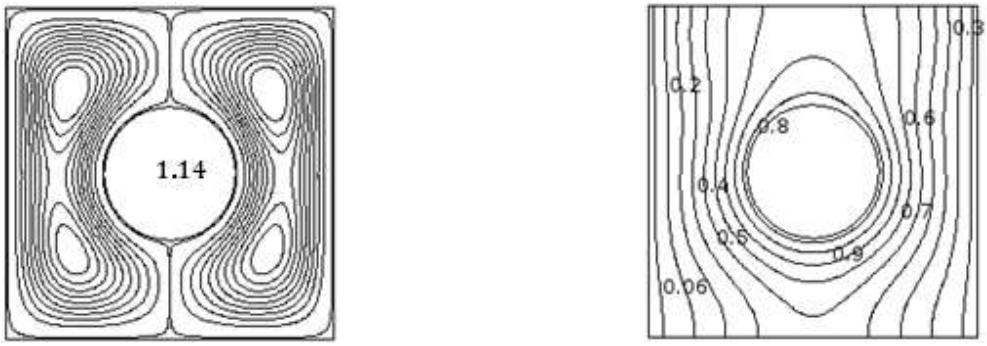

(b) Present study

Figure 2: Comparison of streamlines (left) and isotherms (right) contours of the present study are in agreement with those of the benchmark problem of Hussein [29].

Figure 3: Comparison of streamlines (left) and isotherms (right) of the present study are in agreement with those of the benchmark problem of Chamkha and Ismael [4].

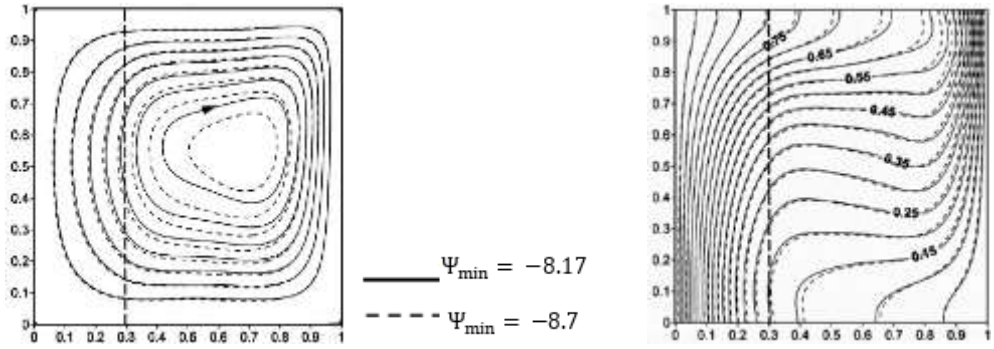

(a) Chamkha and Ismael [4]

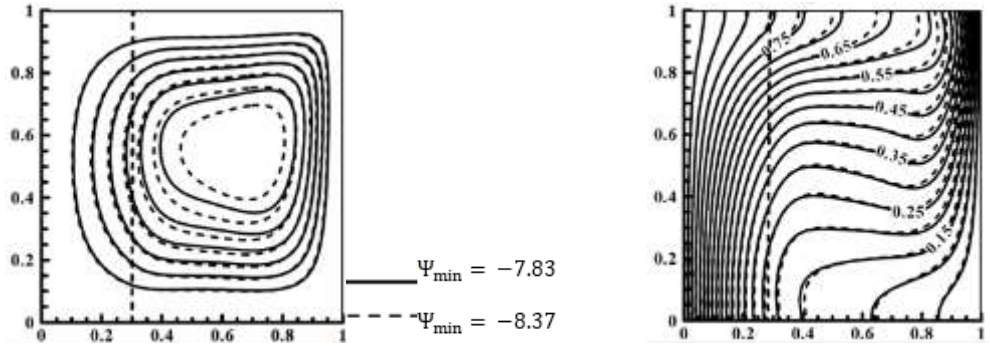

(b) Present study

3.2 Grid independent test.

Figure 4 shows the grid of the two-dimensional domain using unstructured tetrahedral cells. The mesh nearby the interface between the fluid and porous layers and the enclosure boundaries are refined to capture the variables. The grid of the domain is performed for a hollow corrugated enclosure partly filled with a porous medium slab saturated with a

nanofluid and the reminder part of the enclosure filled with the same type of nanofluid. The grid tests were implemented at Ra = 10^6, Da = 10^{-3}, X_p = 0.2, Am = 0.2, λ = 3, R_k = 1and ϕ = 0.1. The selected number of elements 19,753 was used to assess the accuracy and the analysis cost of the numerical procedure because of the convergence value of the average Nussult number was started at this value of the number of elements as shown in Figure 5.

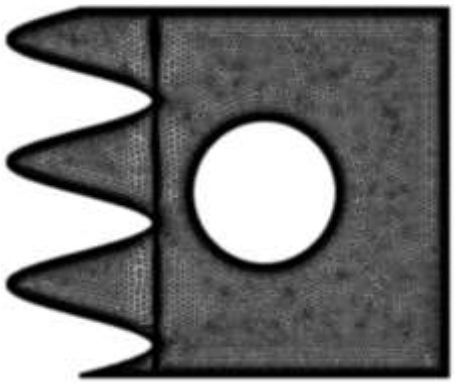

Figure 4: Non-dimensional computational refined mesh of the physical domain.

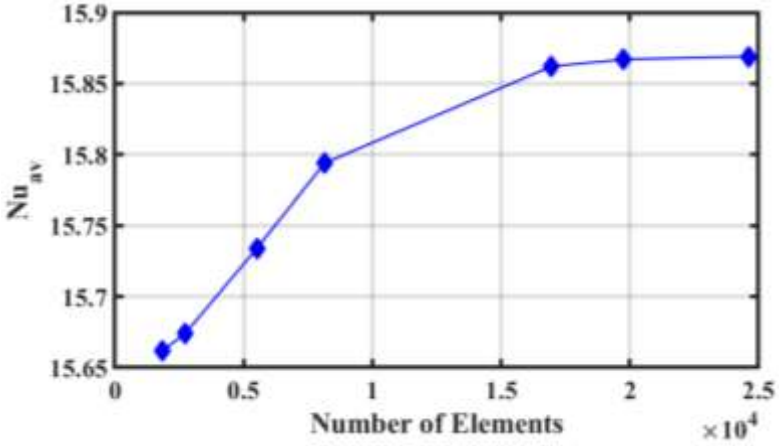

Figure 5: Independent grid test between the average Nusselt number and number of elements.

4. Results and Discussion

In this section, the outcomes of the numerical simulation were determined for the streamline and isotherm contours and as graphical profiles of the local and average Nusselt numbers at the cylinder surface against various selected effective parameters. In all Figures of isotherm line contours, the temperature distribution was a maximum value at the cylinder's surface and its value reduced to a minimum value at the enclosure boundaries. The ranges of the simulation parameters in this study are: the Rayleigh number (Ra), $10^4 \leq Ra \leq 10^6$, the Darcy number (Da), $10^{-5} \leq Da \leq 10^{-1}$, the porous layer thickness (X_p), $0.2 \leq X_p \leq 1$, , the thermal conductivity ratio of porous/nanofluid layers (Rk), $0.1 \leq Rk \leq 100$, the wave number (frequency) (λ), $1 \leq \lambda \leq 3$, the wave amplitude (Am), $0.1 \leq A_m \leq 0.2$, and the nanoparticle volume fraction (ϕ), $0 \leq \phi \leq 0.1$. Generally, and according to the boundary conditions, the fluid close to the heated circular cylinder rises towards the upper cold wall of the enclosure as a results of the density variation (buoyancy effect). The fluid moved at different velocities due to the flow resistance produced by the porous layer. Thereafter, the flow direction descent along the right and left cooled walls of the enclosure in the fluid and porous layers and this led to generating two asymmetric vortices. The isotherm contours are graduated inside the enclosure as a higher temperature at the cylinder surface and a lower temperature at the enclosure boundaries.

4.1 Streamlines and isotherms:

Figure 6 shows the effect of porous layer thickness (Xp) on the streamlines at Ra = 10^6, Da = 10^{-3}, Am = 0.1, λ = 1, Rk = 1, and ϕ = 0.1. At Xp = 0.2, a strong primary vortex (Ψ_{max} = - 28) in a clockwise flow direction passes around the right half of the circular cylinder at an angle from $-\pi/2$ to $\pi/2$ and covers the fluid layer, while a weak secondary vortex (Ψ_{min} = 19.5) in an anti-clockwise flow direction occupies the second half of the cylinder under the effects of the porous layer and the corrugated wall of the enclosure. The pole centres of the primary and secondary vortices are located above the heated cylinder inside the fluid layer with an oval shape. The clustering of the streamlines of the primary and secondary vortices within the fluid layer is higher than that of the streamlines clustering of the secondary vortex at the porous layer due to the flow resistance by the porous matrix. The stream function strength of the secondary vortex significantly decreases as the porous layer thickness increases to 0.3. This is due to increasing the porous layer area and moving the pole centre of the secondary vortex close to

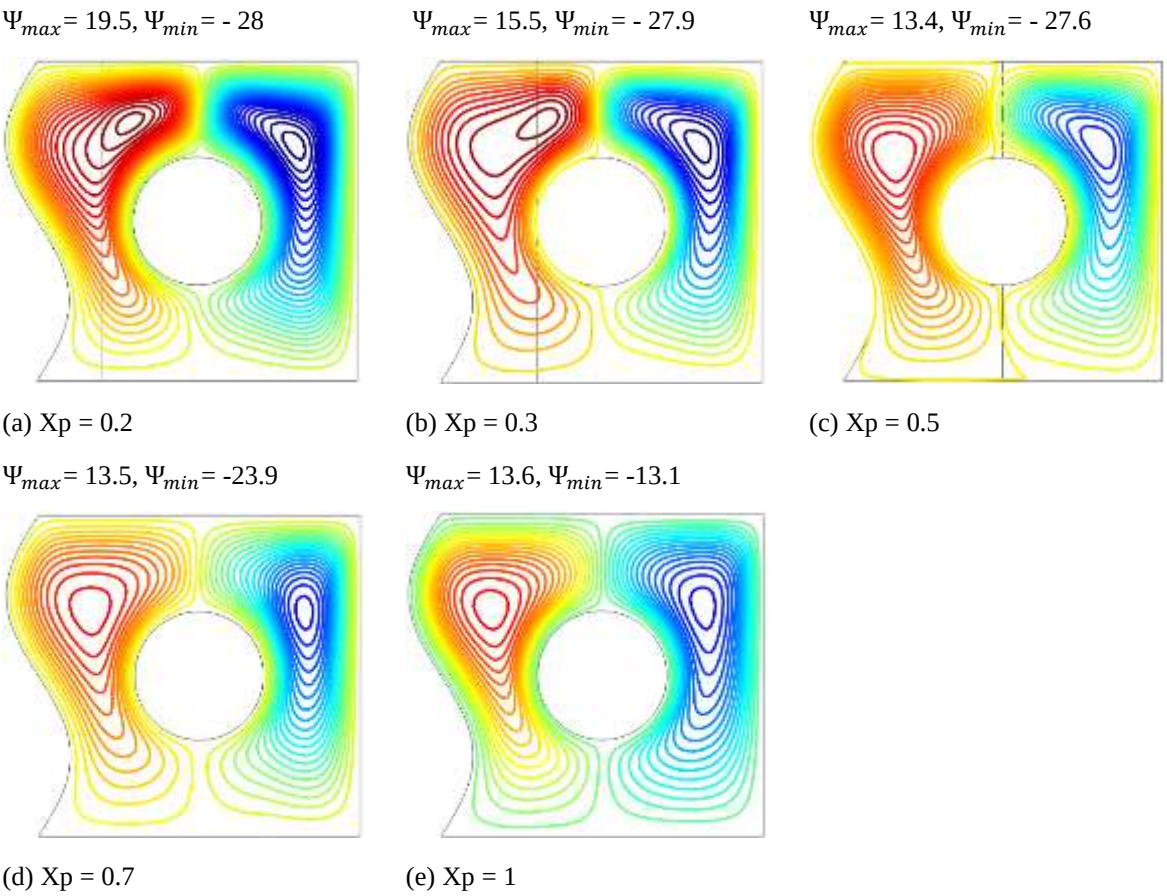

Figure 6: Contour maps of the streamlines for different porous layer thickness using Ra = 10^6, Da = 10^{-3}, Am = 0.1, λ = 1, Rk = 1, and ϕ = 0.1.

the interface line between the porous and fluid layers. Higher porous layer thickness (0.5 - 0.7) leads to occupying the pole centres inside the fluid layer and porous layer with a significant reduction in the stream function strength and causing a compression of the secondary vortex inside the fluid layer. At Xp = 1, a noticeable increase of the stream function strength of the secondary vortex (Ψ_{min} = 13.6) is recorded compared to the primary vortex (Ψ_{max} = -13.1). This stems from the accelerated flow and narrow area generated by the corrugated left wall of the enclosure.

In Figure 7, the isotherms prediction shows that the isotherm lines around the heated circular cylinder are more clustered at Xp = 0.2 compared to other values of Xp. In addition, the diagonal pattern of the isotherms in the porous layer indicates the conductive heat transfer, while the horizontal pattern in the fluid layer indicates the convective heat transfer. Increasing the porous layer thickness lead to moving the plume of the isotherm lines above the cylinder from the nanofluid layer towards the porous layer. The heat diffusion from the inner heated

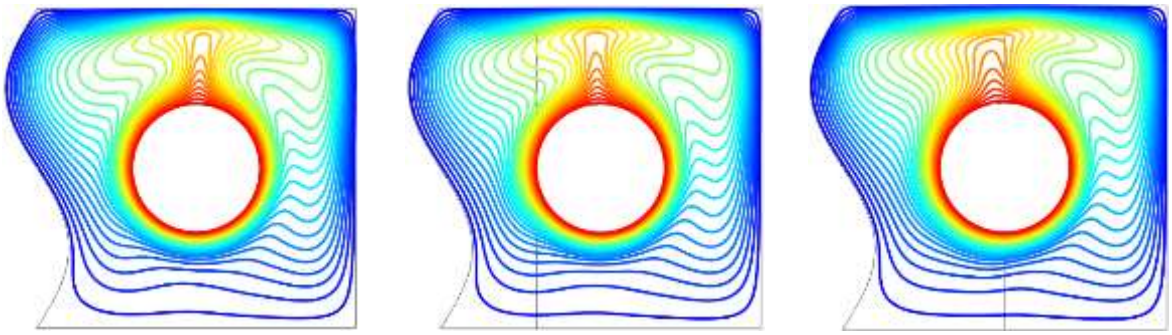

(a) Xp = 0.2 (b) Xp = 0.3 (c) Xp = 0.5

(d) Xp = 0.7 (e) Xp = 1

Figure 7: Contour maps of the isotherms for different porous layer thickness using Ra = 10^6, Da = 10^{-3}, Am = 0.1, λ = 1, R_k = 1, and ϕ = 0.1.

cylinder inside the enclosure decreases with increasing the porous layer thickness more than 0.2.

The prediction of the streamlines and the isotherms for different values of Rayleigh number and Darcy number at Xp = 0.5, Am = 0.1, λ = 1, Rk = 1 and ϕ = 0.1 is illustrated in Figures 8 and 9. In Figure 8, at Ra = 10^4 and Da = 10^{-5}, the core center of the secondary vortex inside the porous layer with an egg shape confines between the cylinder and the corrugated wall of the enclosure at an angle from $\pi/2$ to 3 $\pi/2$. A low stratification of the streamlines of the secondary vortex appeares within the porous layer compared to the primary vortex within the fluid layer due to the flow resistance by the porous slab and the low value of the Darcy number. The primary vortex within the fluid layer has two poles close to the cylinder surface that are located at angles from 0 to $\pi/2$ and 0 to - $\pi/2$ with a higher strength of the stream function compared to the secondary vortex. Increasing the Darcy number to 10^{-3} and 10^{-1} leads to increasing the penetration and the streamlines strength of the secondary vortex with a constant strength of the streamlines for the primary vortex. At Da = 10^{-1}, the strength of the secondary vortex within the porous layer is relatively higher than the primary vortex in the fluid layer due to extending the core centre of the secondary vortex as an egg shape toward the interface line between the

Figure 8:

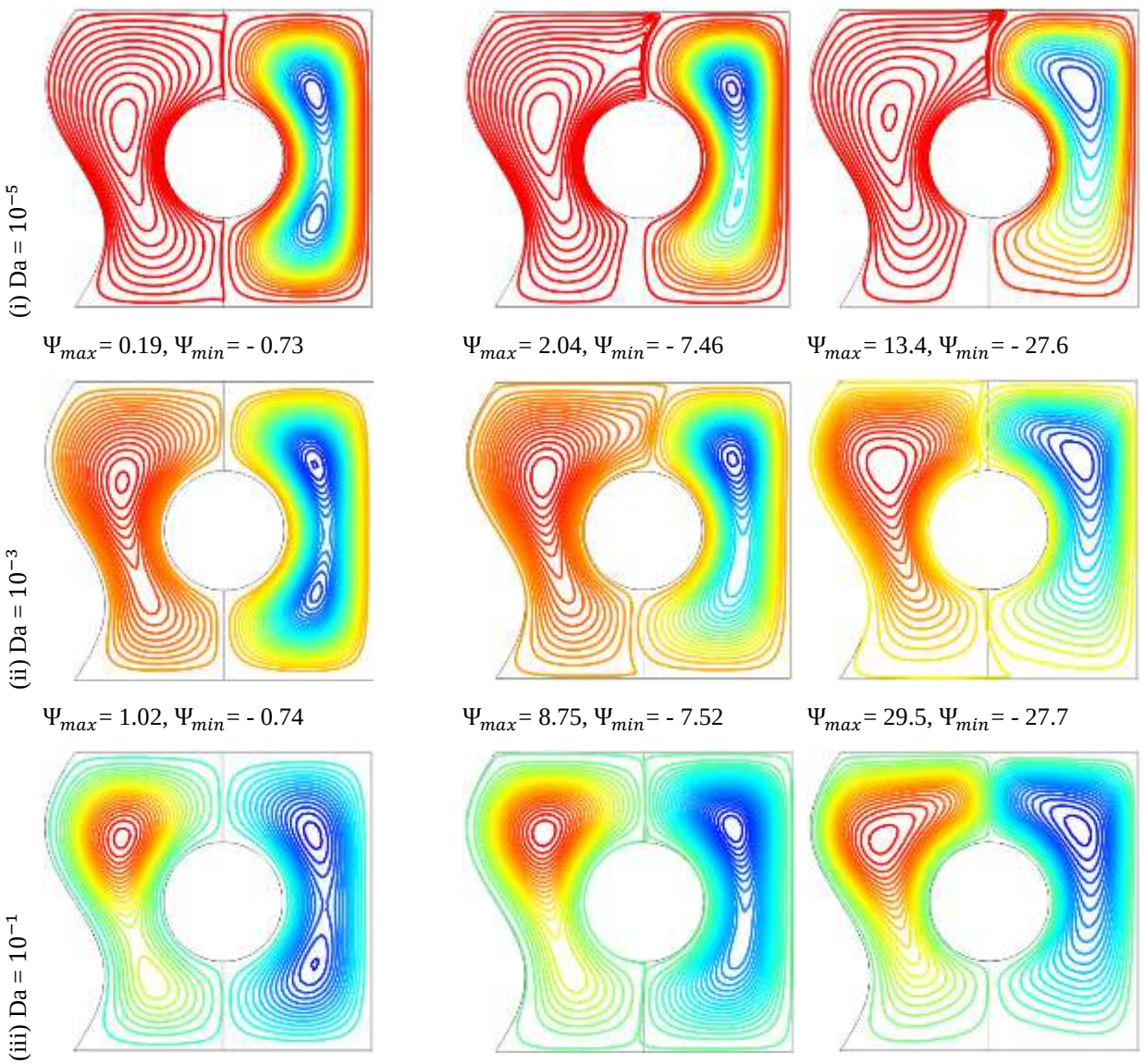

Streamlines at different values of Darcy numbers using Xp = 0.5, Am = 0.1, λ = 1, Rk = 1 and ϕ = 0.1 at (a) Ra =10^4,(b) Ra =10^5 and (c) Ra =10^6.

porous layer and fluid layer beside the accelerated flow due to the narrow area generated by the corrugated left wall of the enclosure.

A direct relationship between the strength of the convective flow and the maximum and minimum values of the stream function is predicted. Increasing the Rayleigh number leads to increasing the strength of the stream function and hence the convective flow strength. This act leads to a uniform distribution of the isotherm lines inside the enclosure around the heated circular cylinder at Ra= 10^4 for all values of Darcy number as shown in Figure 9. The isotherm lines are clustered around the heat source and extending a plume of these lines from the heat

source towards the upper and vertical walls of the enclosure with increasing the Rayleigh number Ra $\geq 10^5$. It is interesting to note that at Ra = 10^6, the clustering of the streamlines within the fluid layer is higher than that of the porous layer at Da = 10^{-5}, while this clustering increases with increasing the Darcy number up to 10^{-1}. This attributes to the dominance of the convective heat transfer mode at the high values of Ra and Da numbers compared to the lower values of these parameters that satisfy the conductive heat transfer mode. This stems from that the higher Rayleigh number and Darcy number resulting in a greater buoyancy force and more permeability of the porous layer producing a higher strength of the stream function and thus increasing the heat removed from the heat source.

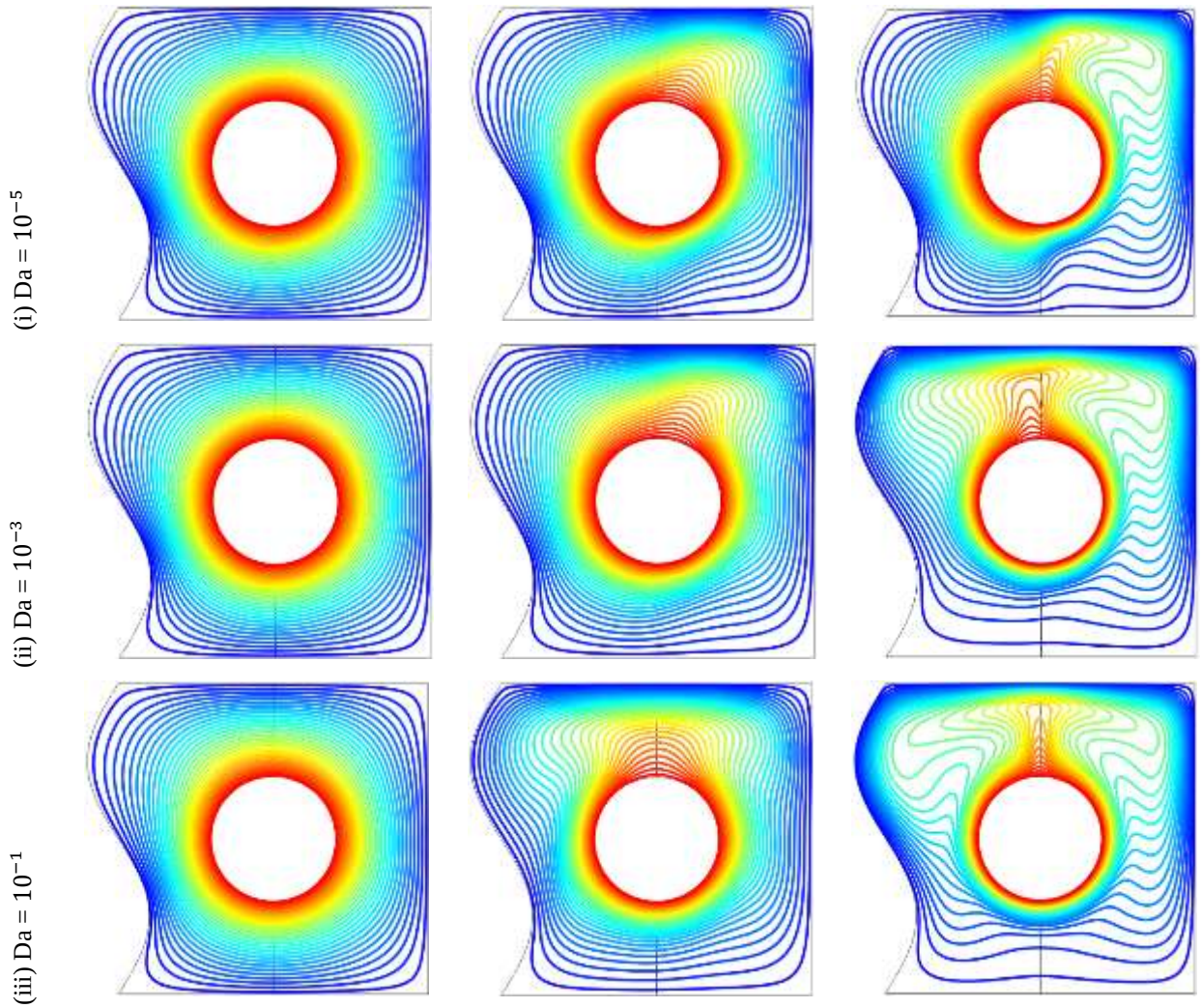

Figure 9: Isotherms at different values of Darcy numbers using Xp = 0.5, Am = 0.1, λ = 1, Rk = 1 and ϕ = 0.1 at (a) Ra =10^4,(b) Ra =10^5 and (c) Ra =10^6.

Figures 10 and 11 show the effect of the wave frequency (λ) of the corrugated wall on the streamlines and the isotherms using Ra = 10^4, Da = 10^{-3}, Xp = 0.5, Rk = 1 and ϕ = 0.1 at (a) Am = 0.1, (b) Am = 0.15 and (c) Am = 0.2. Figure 10 shows that at constant A_m, increasing the wave frequency leads to a compression of the secondary vortex inside the porous layer towards the cylinder and the formation of multi poles with a semi-circle shape whose centres are located close to the heated cylinder except in the case of Am = 0.2 and λ = 2, where the upper circulation core of the secondary vortex has an egg shape and is subjected to a higher relative compression towards the heated cylinder and an extension through the fluid layer

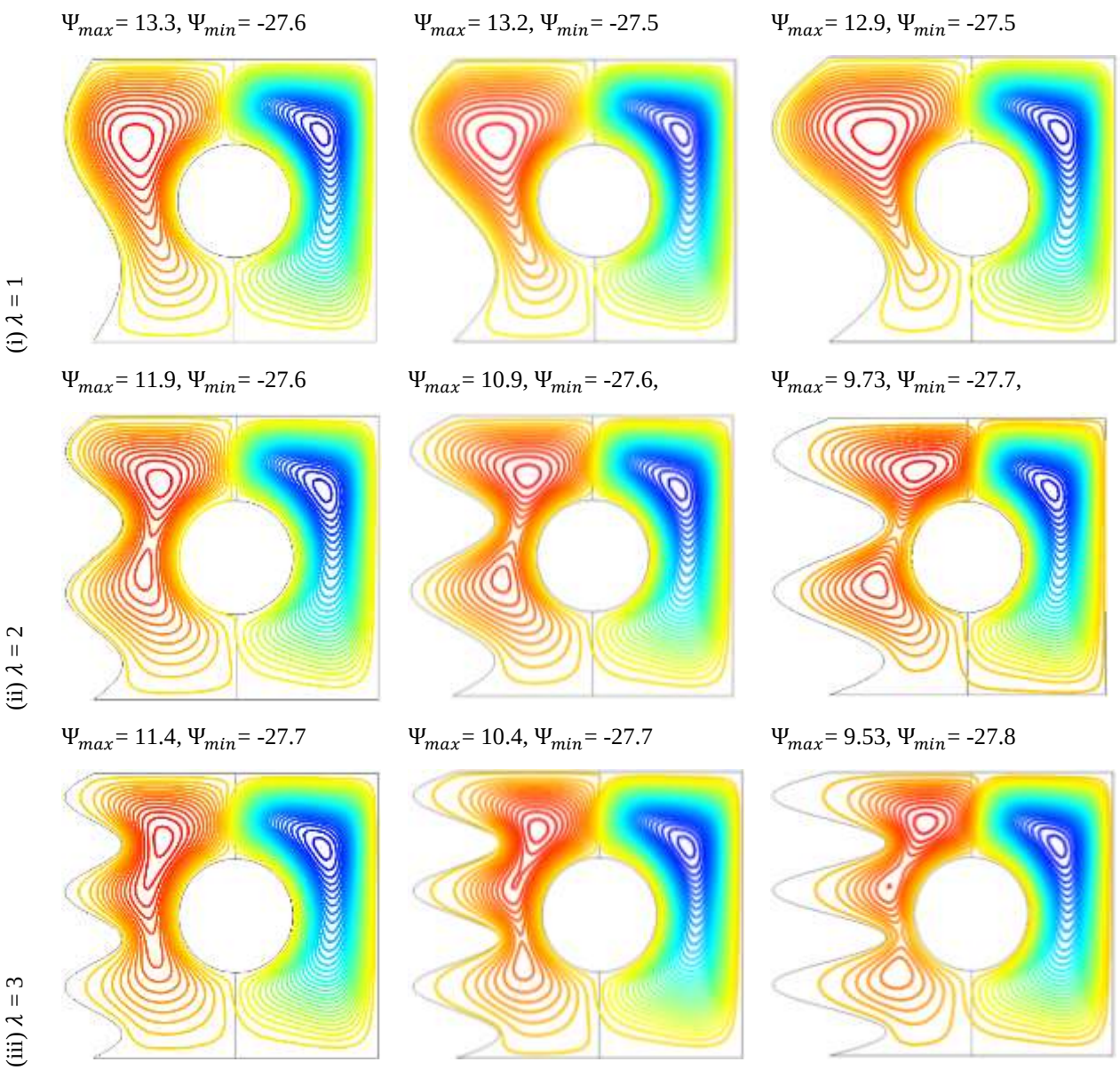

Figure 10: Streamlines at different values of wave frequency when Ra = 10^6, Da = 10^{-3}, Xp = 0.5, Rk = 1 and ϕ = 0.1 at (a) Am = 0.1, (b) Am = 0.15 and (c) Am = 0.2.

Figure 11:

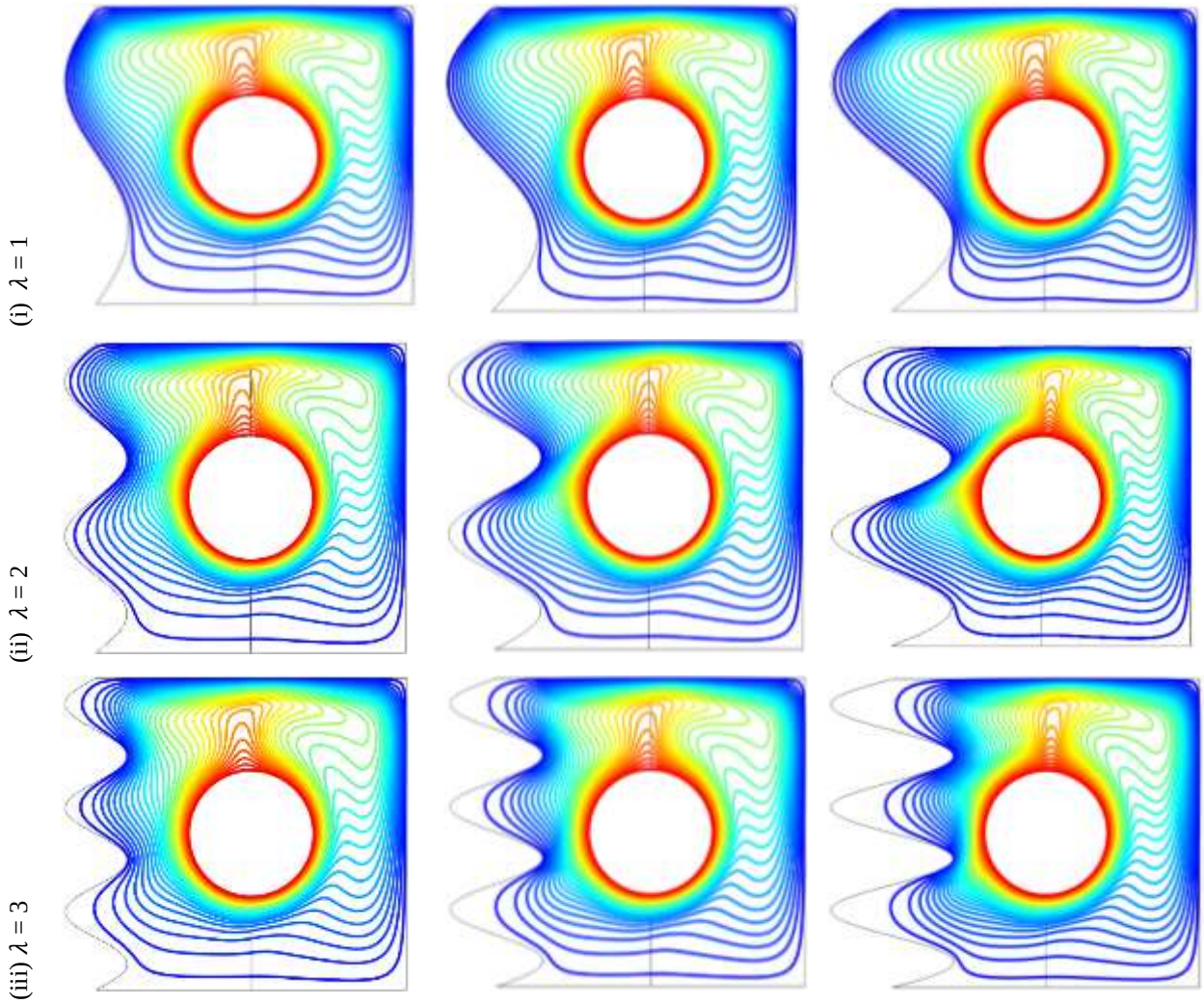

(a) Am = 0.1 (b) Am = 0.15 (c) Am = 0.2

Isotherms at different values of wave frequency when Ra = 10^6, Da = 10^{-3}, Xp = 0.5, Rk = 1 and ϕ = 0.1 at (a) Am = 0.1, (b) Am = 0.15 and (c) Am = 0.2.

compared to other cases. The core centre of the secondary vortex inside the porous layer is closer to the heated cylinder at Am = 0.1 and 0.2 compared to Am = 0.15 due to the curvature effect of the corrugated wall for different values of λ. There is no significant variation in the strength of the primary vortex inside the fluid layer with increasing the wave frequency while there is a noticeable decrease in the strength of the secondary vortex with increasing the wave frequency, especially from λ = 1 to λ = 2. Increasing the wave amplitude results in a relative decrease in the strength of the stream function of the secondary vortex for all values of λ. The temperature distribution inside the enclosure shows that the horizontal pattern of the isotherm lines in the fluid layer refers to the convective heat transfer, while the diagonal pattern in the porous layer expresses the conductive heat transfer as shown in Figure 11. The clustering of the isotherm lines when Am = 0.1 is higher than that at Am = 0.15. This is due to the higher strength of the stream function of the secondary vortex at Am = 0.1. Increasing the wave amplitude leads to moving the plume of the isotherm lines above the cylinder from the porous layer towards the fluid layer for all values of the wave frequency. At Am = 0.2 for different values of λ and especially at λ = 2, a significant clustering of the isotherm lines occurs around the heated cylinder as well as a thinner plume of the isotherm lines appears at the upper surface of the cylinder. This stems from the fact that the poles' centres of the secondary vortex are closer to the heated cylinder compared to the locations of the poles' centres of the secondary vortex for the other values of Am.

4.2 Heat transfer rate: Local Nusselt number (Nul)

Figure 12 shows the predictions of the local Nusselt number on the heated circular cylinder under the different effects of selected parameters such as Rayleigh number (a), Darcy number (b), porous medium thickness (c) and the wave amplitude (d).

Figure 12a illustrates the variation of the local Nusselt number with Rayleigh number on the circular cylinder at Da = 10^{-3}, Xp = 0.5, Am = 0.1, λ = 1, R_k = 1, and ϕ = 0.1. The local Nusselt number increases with increasing Ra due to increasing the strength of the stream function for both the primary and secondary vortices. At any value of the Rayleigh number, there is a gradual increase of the local Nusselt number until it reaches a maximum value at a location on the cylinder surface is 0.4 (4π/5). Thereafter, a gradual decline occurs in its value at a location on the cylinder surface from 0.4(4π/5) to1(2π). This attributes to the effect of the core centres' locations of the primary and secondary vortices at the upper surface of the cylinder inside the fluid layer and porous layer, respectively. In addition, the strength of the stream function of the secondary vortex in the porous layer is higher than that of the primary vortex in the fluid layer. It is interesting to note that there is an inverse behaviour of the local Nusselt number at a location on the cylinder surface almost from 0.75(3π/2) to 1(2π) due to the formation of a second pole of the primary vortex at Ra = 10^4 compared to the other values of Rayleigh number as shown in Figure 8(ii). There is no appreciable effect of the local Nusselt number at Ra = 10^4. This is because of the low value of the stream function strength for both the primary and secondary vortices compared to the other values of Ra.

The variation of the local Nusselt number along the cylinder surface for different Darcy numbers at Ra = 10^6, Xp = 0.5, Am = 0.1, λ = 1, R_k = 1, and ϕ = 0.1 is illustrated in Figure 12b. The local Nusselt number increases with increasing the Darcy number due to increasing the permeability of the porous medium, where increasing the Darcy number causes a reduction in the resistance offered by the porous layer to the nanofluid flow. It gradually increases to its maximum value at a location on the surface cylinder from 0 to 0.4 (4π/5). Thereafter, it gradually declines up to the location of the surface cylinder that is equal to 1(2π) for different values of Da. This is due to the effect of the core centres' locations of the primary and secondary vortices at the upper surface of the cylinder inside the fluid layer and porous layer, respectively. In addition, the strength of the stream function of the secondary vortex in the porous layer is higher than that of the primary vortex in the fluid layer.

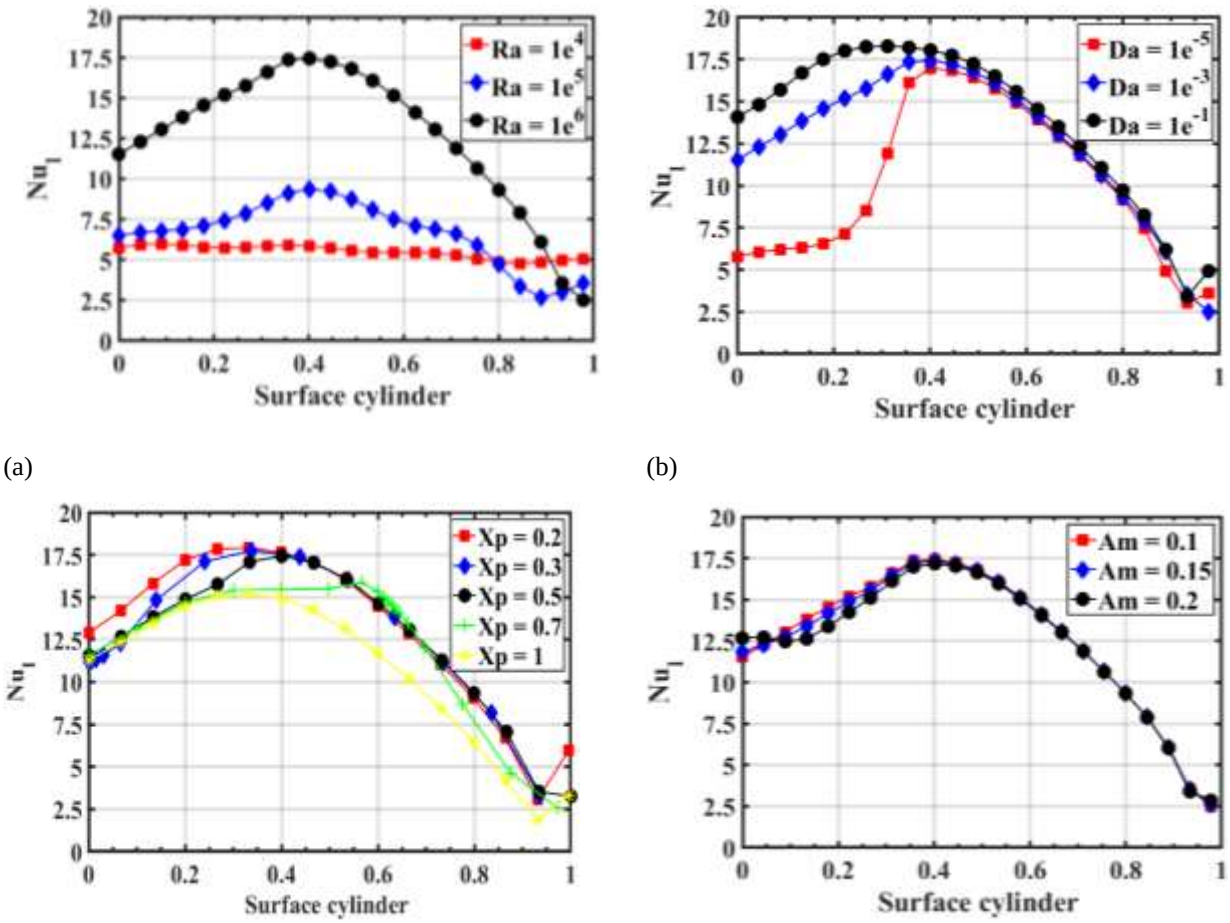

Figure 11: Variation of the local Nusselt number along the heat source (surface cylinder) with different dimensionless parameters (a) Ra effect, (b) Da effect, (c) Xp effect and (d) Am effect.

Figure 11c depicts the effect of the porous medium thickness on the local Nusselt number along the heated cylinder surface at Ra = 10^6, Da = 10^{-3}, Am = 0.1, λ = 1, R_k = 1, and ϕ = 0.1. It seems that the local Nusselt number gradually increases with decreasing the porous layer thickness. This is because at lower values of Xp, the resistance area of the porous matrix decreases, which leads to an augmentation of convective heat transport within the nanofluid layer compared to the porous layer. A maximum value of local Nusselt number satisfies at a location on the surface cylinder from 0 to 0.4 ($4\pi/5$). A gradual decrease in the local Nusselt number value occurs up to the location of the surface cylinder equal to 1(2π) for different values of Xp. This is due to the effect of the core centres' location of the primary and secondary vortices at the upper surface of the heated cylinder. In addition, increasing the porous layer thickness causes to decrease in the strength of the stream function. This increase leads to moving the core centre of the secondary vortex and the plume of the isotherm lines from the nanofluid layer toward the porous layer as shown in Figures 6 and 7.

The variation of the local Nusselt number along the heated cylinder surface with different wave amplitude at Ra = 10^6, Da = 10^{-3}, Xp = 0.5, λ = 1, R_k = 1, and ϕ = 0.1 is shown in Figure 11d. At location 0 on the cylinder surface, the local Nusselt number increases with increasing the wave amplitude. This pattern takes an opposite trend up to 0.4($4\pi/5$) on the cylinder surface due to the relatively moving of the core centre of the secondary vortex away from the cylinder inside the porous layer under the effect of increasing the convexity of the corrugated wall. A gradual decline occurs in the local Nusselt number after the location of 0.4($4\pi/5$) at the cylinder surface. There is no appreciable effect of increasing the wave amplitude on the local Nusselt number. This attributes to the location of the core centres of the primary and secondary vortices at the upper surface of the heated cylinder.

4.3 Heat transfer rate: Average Nusselt number (Nu_{av})

Figure 12 shows the variation of the average Nusselt number (Nu_{av}) versus the logarithmic values of Darcy number for different values of (a) nanoparticles volume fraction, (b) Rayleigh number and (c) thermal conductivity ratio.

Figure 12a shows the relationship between Nu_{av} versus the logarithmic values of Da for various nanoparticles volume fraction values as Ra = 10^6, Xp = 0.5, Am = 0.1, λ = 1and R_k = 1. It seems that increasing the nanoparticles volume fraction causes to increase Nu_{av}. This stems from the fact that adding the nanoparticles to the pure fluid leads to improving the thermal

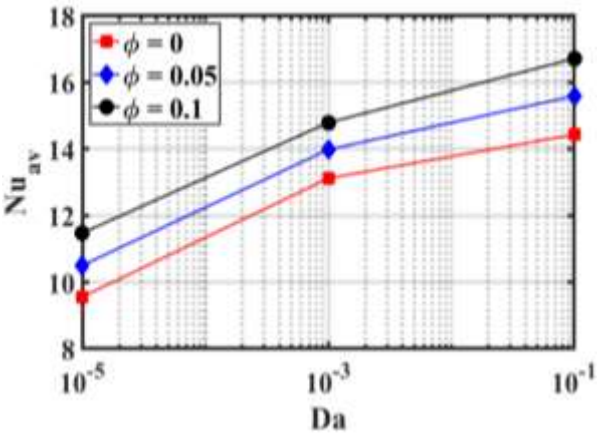

(a)

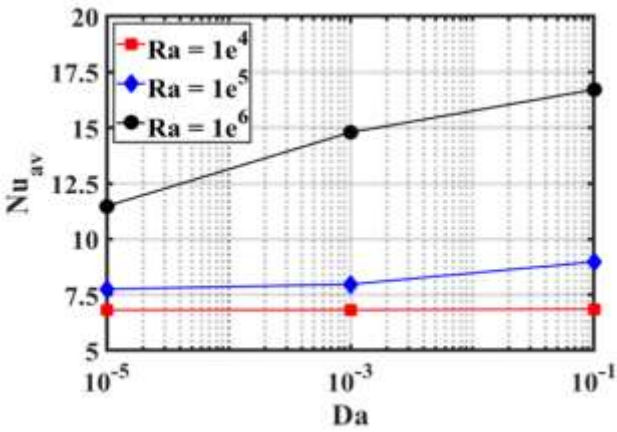

(b)

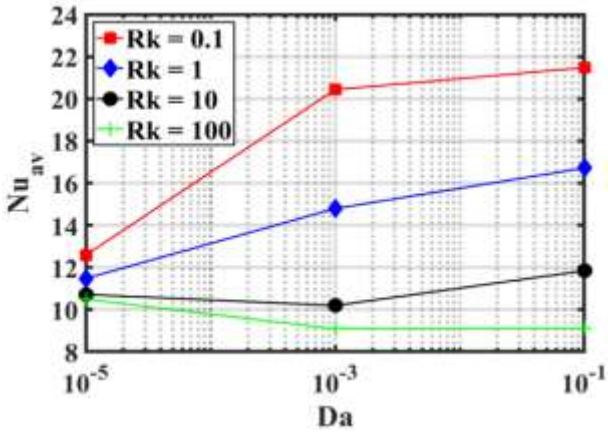

(c)

Figure 12: Variation of average Nusselt number versus the Darcy number for different dimensionless parameters (a) ϕ effect, (b) Ra effect and (c) Rk effect.

conductivity and thus enhancing the convective heat transfer. It is interesting to note that at the lower value of the Darcy number Da = 10^{-5}, which causes to increase in the resistance offered by the porous matrix, the reduction in Nuav due to the decreased Darcy number can be overcome by increasing the nanoparticle volume fraction.

The variation of Nu_{av} versus the logarithmic values of Da for different values of the Rayleigh number as Xp = 0.5, Am = 0.1, λ = 1, R_k = 1 and ϕ = 0.1is shown in Figure 12b. This Figure shows that Nu_{av} gradually increases with increasing the value of Ra. A significant increase of Nu_{av} with increasing Ra for different Da values due to increasing the buoyancy force and the strength of the stream function (see Figure 8c), while there is no appreciable effect of Nu_{av} at Ra = 10^4. At Da = 10^{-5}, the minimum values of Nu_{av} are recorded for different values of Ra. This attributes to the flow resistance offered by the porous matrix as well as the decrease in the streamlines strength as shown in Figure 8(i).

The effect of increasing the thermal conductivity ratio (Rk) on the variation of Nu_{av} versus the logarithmic values of Da as Ra = 10^6, Xp = 0.5, Am = 0.1, λ = 1 and ϕ = 0.1 is illustrated in Figure 12c. At Da = 10^{-5}, the low values of Nu_{av} attributes to the flow resistance offered by the porous matrix as well as the decrease in the streamlines strength inside the porous layer (not fixed as contours). At

lower values of Rk (1 and 0.1), Nu_{av} increases with increasing the logarithmic values of Da due to the increase of the streamlines strength in the primary and secondary vortices beside the effect of the left corrugated wall of the enclosure. A significant decrease in Nu_{av} values are recorded at Rk =10 and 100 due to moving the core centers of the primary and secondary vortices away from the heated circular cylinder. Generally, the lower value of Rk produces higher rates of heat transfer for different Darcy numbers.

Figure 13 predicts the variation of the average Nusselt number versus the wave frequency for different wave amplitude when (a) Xp = 0.2, (b) Xp = 0.5, (c) Xp = 0.7 and (d) Xp = 1 as Ra =

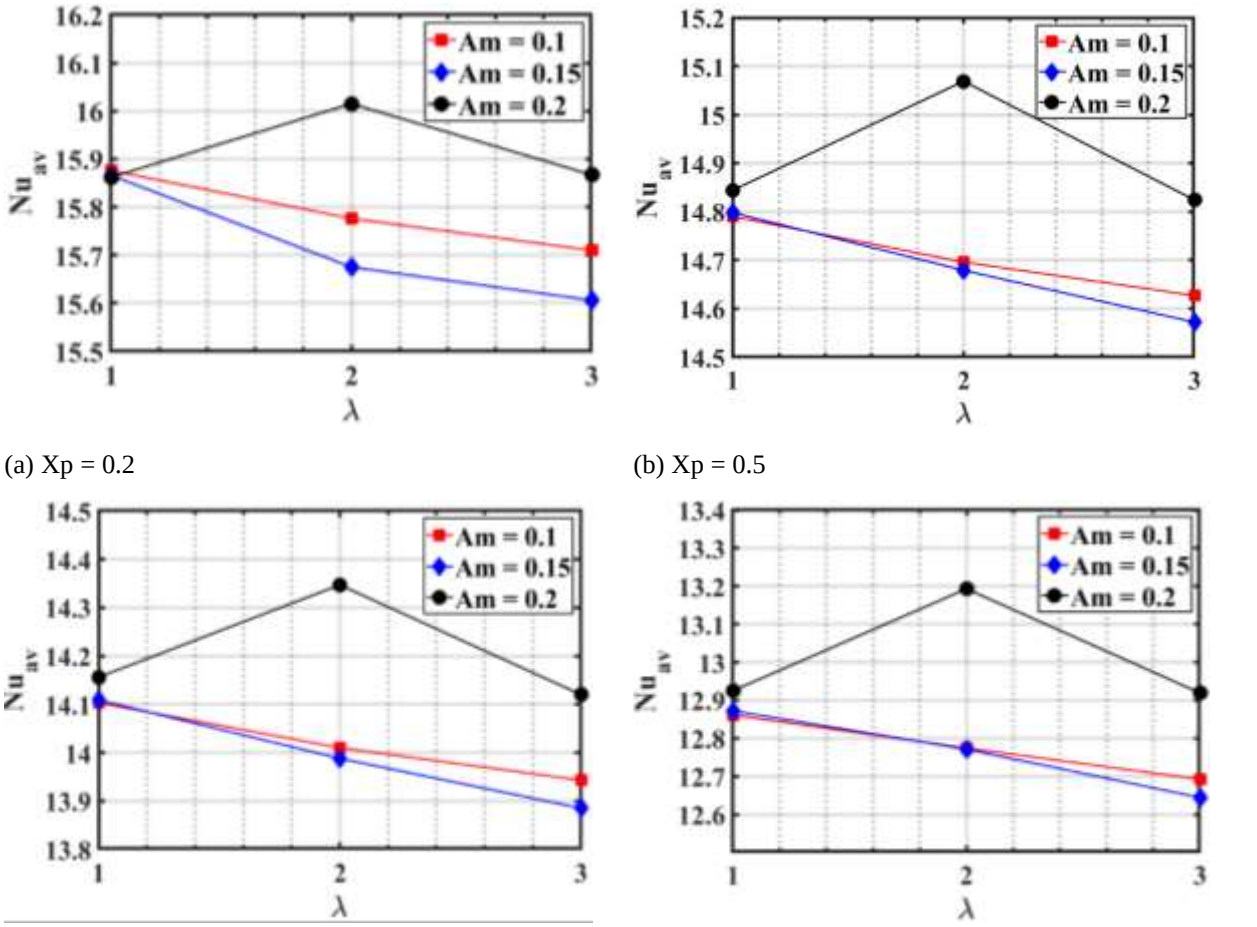

(a) Xp = 0.2 (b) Xp = 0.5

(c) Xp = 0.7 (d) Xp = 1

Figure 13: Variation of average Nusselt number versus the wave frequency for different wave amplitudes at (a) Xp = 0.2, (b) Xp = 0.5, (c) Xp = 0.7 and (c) Xp = 1.

10^6, Da = 10^{-3}, R_k = 1, and ϕ = 0.1. It seems that increasing the porous layer thickness produces a significant decrease in Nu_{av} values for different values of Am and λ. This is due to increasing the resistance area offered by the porous matrix and decreasing the streamlines strength at both the primary and secondary vortices as shown in Figure 6. At constant Xp, Nu_{av} decreases with increasing Am from 0.1 to 0.15. This is due to moving the poles of the secondary vortex away from the heated cylinder producing a decrease in the streamlines strength. This is due to the two poles' location of the secondary vortex which is closer to the heated cylinder beside the corrugated wall effect compared to the other values of λ and Am as shown in Figure 10. Increasing λ to 3 causes to decrease in the heat transfer rates for all Am values. This is because of the formation of the three poles at the secondary vortex with a low strength of the stream function compared to λ = 1 and 2.

5. Conclusions

Steady-state natural convection flows inside an enclosure partly filled with a porous slab saturated with Ag-water nanofluid under the effects of an inner circular cylinder and a left vertical corrugated wall have been numerically studied. The enclosure is uniformly heated with a constant temperature, Th at the surface of the inner cylinder fixed at the enclosure centre and cooled at the enclosure

walls with a constant temperature, Tc. The porous slab is located on the left close to the vertical corrugated wall while the fluid layer is located on the right close to the vertical flat wall. The nanofluid was composed of water-containing Ag nanoparticles. The ranges of the simulation parameters in this study are: the Rayleigh number (Ra), $10^4 \leq Ra \leq 10^6$, the Darcy number (Da), $10^{-5} \leq Da \leq 10^{-1}$, the porous layer thickness (X_p), $0.2 \leq X_p \leq 1$, , the thermal conductivity ratio of porous/nanofluid layers (Rk), $0.1 \leq Rk \leq 100$, the wave number (frequency) (λ), $1 \leq \lambda \leq 3$, the wave amplitude (Am), $0.1 \leq A_m \leq 0.2$, and the nanoparticle volume fraction (ϕ), $0 \leq \phi \leq 0.1$. The obtained results of this study are summarized in the following conclusions:

- Due to the uniformly heated inner circular cylinder and the uniformly cooled enclosure walls, two vortices were generated at the fluid and porous layers. The primary vortex was located in the fluid layer while the secondary vortex was located in the porous layer. The primary vortex rotated in a clockwise direction while the secondary vortex rotated in an anti-clockwise direction.
- A significant increase in the heat transfer rate was recorded with increasing Ra for different Da values due to increasing the buoyancy force and the streamlines strength. Heat transfer rate is enhanced by using the nanofluid compared to the single-phase fluid (water). The lower value of the Darcy number $Da = 10^{-5}$, causes to increase in the resistance offered by the porous matrix; the reduction in heat transfer rate due to the decreased Darcy number can be overcome by increasing the nanoparticle volume fraction.
- The lower value of K_r produced a higher heat transfer rate for different Darcy numbers.
- The heat transfer rate is improved at the lower thickness of the porous layer.
- A significant increase was recorded in the heat transfer rate when $\lambda = 2$ and $Am = 0.2$ due to the formation of two poles for the secondary vortex inside the porous layer closer to the heated cylinder and the corrugated wall effect compared to the other values of λ and Am.

References

[1] T. Basak, S. Roy, A. Matta, and I. Pop, "Analysis of heatlines for natural convection within porous trapezoidal enclosures: Effect of uniform and non-uniform heating of bottom wall," *Int. J. Heat Mass Transf.*, vol. 53, no. 25–26, pp. 5947–5961, 2010, doi: 10.1016/j.ijheatmasstransfer.2010.07.026.

[2] M. A. Al-Nimr and A. F. Khadrawi, "Transient free convection fluid flow in domains partially filled with porous media," *Transp. porous media*, vol. 51, no. 2, pp. 157–172, 2003.

[3] F. Arpino, N. Massarotti, and A. Mauro, "International Journal of Heat and Mass Transfer Efficient three-dimensional FEM based algorithm for the solution of convection in partly porous domains," *Int. J. Heat Mass Transf.*, vol. 54, no. 21–22, pp. 4495–4506, 2011, doi: 10.1016/j.ijheatmasstransfer.2011.06.030.

[4] A. J. Chamkha and M. A. Ismael, "Natural Convection in Differentially Heated Partially Porous Layered Cavities Filled with a Nanofluid," *Numer. Heat Transf. Part A Appl.*, vol. 65, no. 11, pp. 1089–1113, Jun. 2014, doi: 10.1080/10407782.2013.851560.

[5] R. A. Mahdi, H. A. Mohammed, and K. M. Munisamy, "Improvement of Convection Heat Transfer by Using Porous Media and Nanofluid : Review," vol. 2, no. 8, 2013.

[6] D. A. Nield and A. Bejan, *Convection in porous media*, vol. 3. Springer, 2006.

[7] V. Kumar, "Coupling of free flow and flow in porous media–a dimensional analysis," *Forschungsbericht, Inst. für Wasserbau, Lehrstuhl für Hydromechanik und Hydrosystemmodellierung, Univ. Stuttgart*, 2011.

[8] A. Bagchi and F. A. Kulacki, *Natural convection in superposed fluid-porous layers*. Springer, 2014.

[9] J. M. Medeiros, F. Marcondes, and J. M. Gurgel, "Natural convection in a porous cavity using the generalized model with uniform porosity," 1999.

[10] A. K. Tiwari, A. K. Singh, P. Chandran, and N. C. Sacheti, "Natural convection in a cavity with a sloping upper surface filled with an anisotropic porous material," *Acta Mech.*, vol. 223, no. 1, pp. 95–108, 2012.

[11] A. Fard, B. Ghasemi, and M. Kohyani, "Heat generation effects on natural convection in porous cavity with different walls temperature," *Front. Heat Mass Transf.*, vol. 3, no. 2, 2012.

[12] F. Wu, G. Wang, and W. Zhou, "Buoyancy induced convection in a porous cavity with sinusoidally and partially thermally active sidewalls under local thermal non-equilibrium condition," *Int. Commun. Heat Mass Transf.*, vol. 75, pp. 100–114, 2016, doi: 10.1016/j.icheatmasstransfer.2016.03.026.

[13] A. I. Alsabery, A. J. Chamkha, I. Hashim, and P. G. Siddheshwar, "Effects of Nonuniform Heating and Wall Conduction on Natural Convection in a Square Porous Cavity Using LTNE Model," *J. Heat Transfer*, vol. 139, no. 12, pp. 1–13, 2017, doi: 10.1115/1.4037087.

[14] T. Basak, S. Roy, and H. S. Takhar, "Effects of nonuniformly heated wall(S) on a natural-convection flow in a square cavity filled with a porous medium," *Numer. Heat Transf. Part A Appl.*, vol. 51, no. 10, pp. 959–978, 2007, doi: 10.1080/10407790601128600.

[15] M. A. Ismael and A. J. Chamkha, "Conjugate natural convection in a differentially heated composite enclosure filled with a nanofluid," *J. Porous Media*, vol. 18, no. 7, 2015.

[16] A. I. Alsabery, A. J. Chamkha, S. H. Hussain, H. Saleh, and I. Hashim, "Heatline visualization of natural convection in a trapezoidal cavity partly filled with nanofluid porous layer and partly with non-Newtonian fluid layer," *Adv. Powder Technol.*, vol. 26, no. 4, pp. 1230–1244, 2015, doi: 10.1016/j.apt.2015.06.005.

[17] B. M. Al-Srayyih, S. Gao, and S. H. Hussain, "Effects of linearly heated left wall on natural convection within a superposed cavity filled with composite nanofluid-porous layers," *Adv. Powder Technol.*, vol. 30, no. 1, pp. 55–72, 2019.

[18] B. M. Al-Srayyih, S. Gao, and S. H. Hussain, "Natural convection flow of a hybrid nanofluid in a square enclosure partially filled with a porous medium using a thermal non-equilibrium model," *Phys. Fluids*, vol. 31, no. 4, p. 43609, Apr. 2019, doi: 10.1063/1.5080671.

[19] A. Al-Amiri, K. Khanafer, J. Bull, and I. Pop, "Effect of sinusoidal wavy bottom surface on mixed convection heat transfer in a lid-driven cavity," *Int. J. Heat Mass Transf.*, vol. 50, no. 9–10, pp. 1771–1780, May 2007, doi: 10.1016/J.IJHEATMASSTRANSFER.2006.10.008.

[20] M. A. Ismael, "Natural convection in a wavy porous enclosure heated by an internal circular cylinder," *Al-Qadisiya J. Eng. Sci.*, vol. 4, pp. 310–326, 2011.

[21] A. Sojoudi, S. C. Saha, M. Khezerloo, and Y. Gu, "Unsteady natural convection within a porous enclosure of sinusoidal corrugated side walls," *Transp. porous media*, vol. 104, no. 3, pp. 537–552, 2014.

[22] B. Takabi and S. Salehi, "Augmentation of the heat transfer performance of a sinusoidal corrugated enclosure by employing hybrid nanofluid," *Adv. Mech. Eng.*, vol. 6, p. 147059, 2014.

[23] S. H. Hussain, "Analysis of heatlines and entropy generation during double-diffusive MHD natural convection within a tilted sinusoidal corrugated porous enclosure," *Eng. Sci. Technol. an Int. J.*, vol. 19, no. 2, pp. 926–945, 2016.

[24] A. K. Hussein and S. H. Hussain, "Heatline visualization of natural convection heat transfer in an inclined wavy cavities filled with nanofluids and subjected to a discrete isoflux heating from its left sidewall," *Alexandria Eng. J.*, vol. 55, no. 1, pp. 169–186, 2016.

[25] D. G. Roychowdhury, S. K. Das, and T. Sundararajan, "Numerical simulation of natural convective heat transfer and fluid flow around a heated cylinder inside an enclosure," *Heat mass Transf.*, vol. 38, no. 7, pp. 565–576, 2002.

[26] B. S. Kim, D. S. Lee, M. Y. Ha, and H. S. Yoon, "A numerical study of natural convection in a square enclosure with a circular cylinder at different vertical locations," *Int. J. Heat Mass Transf.*, vol. 51, no. 7–8, pp. 1888–1906, 2008.

[27] S. H. Hussain and A. K. Hussein, "Numerical investigation of natural convection phenomena in a uniformly heated circular cylinder immersed in square enclosure filled with air at different vertical locations," *Int. Commun. Heat Mass Transf.*, vol. 37, no. 8, pp. 1115–1126, Oct. 2010, doi: 10.1016/J.ICHEATMASSTRANSFER.2010.05.016.

[28] C. Butler, D. Newport, and M. Geron, "Natural convection experiments on a heated horizontal cylinder in a differentially heated square cavity," *Exp. Therm. Fluid Sci.*, vol. 44, pp. 199–208, 2013.

[29] A. K. Hussein, "Computational analysis of natural convection in a parallelogrammic cavity with a hot concentric circular cylinder moving at different vertical locations," *Int. Commun. heat mass Transf.*, vol. 46, pp. 126–133, 2013.

[30] Y. M. Seo, J. H. Doo, and M. Y. Ha, "Three-dimensional flow instability of natural convection induced by variation in radius of inner circular cylinder inside cubic enclosure," *Int. J. Heat Mass Transf.*, vol. 95, pp. 566–578, 2016.

[31] R. Roslan, H. Saleh, and I. Hashim, "Effect of rotating cylinder on heat transfer in a square enclosure filled with nanofluids," *Int. J. Heat Mass Transf.*, vol. 55, no. 23–24, pp. 7247–7256, Nov. 2012, doi: 10.1016/J.IJHEATMASSTRANSFER.2012.07.051.

[32] J. Ravnik and L. Škerget, "A numerical study of nanofluid natural convection in a cubic enclosure with a circular and an ellipsoidal cylinder," *Int. J. Heat Mass Transf.*, vol. 89, pp. 596–605, 2015.

[33] A. I. Alsabery, M. A. Ismael, A. J. Chamkha, and I. Hashim, "Numerical Investigation of Mixed Convection and Entropy Generation in a Wavy-Walled Cavity Filled with Nanofluid and Involving a Rotating Cylinder," *Entropy*, vol. 20, no. 9. 2018. doi: 10.3390/e20090664.

[34] A. J. Chamkha, F. Selimefendigil, and M. A. Ismael, "Mixed convection in a partially layered porous cavity with an inner rotating cylinder," *Numer. Heat Transf. Part A Appl.*, vol. 69, no. 6, pp. 659–675, Mar. 2016, doi: 10.1080/10407782.2015.1081027.

[35] S. H. Hussain and M. S. Rahomey, "Comparison of natural convection around a circular cylinder with different geometries of cylinders inside a square enclosure filled with Ag-nanofluid superposed porous-nanofluid layers," *J. Heat Transfer*, vol. 141, no. 2, 2019.

[36] A. K. Hussein, H. K. Hamzah, F. H. Ali, and L. Kolsi, "Mixed convection in a trapezoidal enclosure filled with two layers of nanofluid and porous media with a rotating circular cylinder and a sinusoidal bottom wall," *J. Therm. Anal. Calorim.*, vol. 141, no. 5, pp. 2061–2079, 2020, doi: 10.1007/s10973-019-08963-6.